ResearchGate

See discussions, stats, and author profiles for this publication at: https://www.researchgate.net/publication/5416476

Bubble-Free Operation of a Microfluidic Free-Flow Electrophoresis Chip with Integrated Pt Electrodes

ARTICLE *in* ANALYTICAL CHEMISTRY · JULY 2008

Impact Factor: 5.64 · DOI: 10.1021/ac800275c · Source: PubMed

CITATIONS
41

READS
134

5 AUTHORS, INCLUDING:

Dietrich Kohlheyer
Forschungszentrum Jülich
47 PUBLICATIONS **620** CITATIONS
SEE PROFILE

Jan C T Eijkel
University of Twente
160 PUBLICATIONS **3,728** CITATIONS
SEE PROFILE

Stefan Schlautmann
University of Twente
49 PUBLICATIONS **807** CITATIONS
SEE PROFILE

Richard B M Schasfoort
University of Twente
104 PUBLICATIONS **2,446** CITATIONS
SEE PROFILE

Available from: Richard B M Schasfoort
Retrieved on: 31 January 2016

Anal. Chem. **2008,** *80,* 4111–4118

Bubble-Free Operation of a Microfluidic Free-Flow Electrophoresis Chip with Integrated Pt Electrodes

Dietrich Kohlheyer,* Jan C. T. Eijkel, Stefan Schlautmann, Albert van den Berg, and Richard B. M. Schasfoort

MESA$^+$ Institute for Nanotechnology, University of Twente, P.O. Box 217, 7500AE Enschede, The Netherlands

In order to ensure a stable and efficient separation in microfluidic free-flow electrophoresis (FFE) devices, various methods and chips have been presented until now. A major concern hereby is the generation of gas bubbles caused by electrolysis and the resulting disturbances in the position of the separated analyte lanes. Instable lane positions would lead to a decreased resolution in sample collection over time which certainly would be problematic when incorporating a stationary detector system. In contrast to our previous publications, in which we implemented laborious semipermeable membranes to keep bubbles outside the separation region, here we describe an electrochemical approach to suppress the electrolysis of water molecules and therefore bubble formation. This approach allowed a simpler and additionally a closed chip device with integrated platinum electrodes. With the use of this chip, the successful separation of three fluorescent compounds was demonstrated. Quinhydrone, which is a complex of hydroquinone and *p*-benzoquinone, was added only to the local flow streams along the electrodes, preventing mixing with the separation media and sample. The electrical current was generated via the oxidization and reduction of hydroquinone and *p*-benzoquinone up to a certain limit of the electrical current without gas formation. The separation stability was investigated for the chip with and without quinhydrone, and the results clearly indicated the improvement. In contrast to the device operating without quinhydrone, a 2.5-fold increase in resolution was achieved. Furthermore, separation was demonstrated within tens of milliseconds. This chemical approach with its high miniaturization possibilities offers an interesting alternative, in particular for low-current miniaturized FFE systems, in which large and open electrode reservoirs are not tolerable.

Free-flow electrophoresis (FFE) is the continuous separation of charged analytes injected into a thin carrier medium flowing between two insulating plates with an electrical field applied perpendicular to the flow direction. Components with different electrophoretic mobility are deflected under different angles and are separated into various lanes which can be collected at the device outlet.[1] This separation method has found a permanent position in preparative methods in biochemistry and chemistry for the separation of, e.g., cells, organelles, peptides, proteins, and inorganic and organic compounds. Mostly large scale preparative purpose systems have been developed and applied.[2–4] However, a steadily increasing number of publications on miniaturized FFE have shown that μ-FFE allows for high separation resolution with fewer problems, such as Joule heating, compared with their larger counterparts.[5–12] A known problem in FFE is the gas bubble generation at the electrodes due to electrolysis of water which might lead to a distorted separation or loss of the separation voltage. Several approaches have been presented to solve this problem. In order to avoid bubble formation Lu et al.[13] demonstrated a free-flow electrophoresis chip with integrated gold electrodes. In particular they showed free-flow isoelectric focusing with applied voltages below the electrolysis potential.[13] However, because of the low electrical field strength, this device could be used only for relatively large compounds and also separation times of several minutes were necessary. When bubbles are allowed to form, several technological approaches have been applied in μ-FFE devices to eliminate their influence, e.g., by introducing semipermeable membranes or arrays of bubble-blocking microchannels between the electrode regions and the separation area. For more references and further details, the reader is referred to the review on miniaturized free-flow electrophoresis devices by Kohlheyer et al.[14] For a more broad overview of continuous flow microfluidic separation techniques in general, the reader is referred to the recent review by Pamme.[15] In the paper presented here, a new approach is demonstrated to overcome the problem of electrolysis

* Corresponding author. Dietrich Kohlheyer, e-mail: d.kohlheyer@utwente.nl. Phone: +31 53 489 1051.

(1) Hannig, K. and Heidrich, H. G. *Free-Flow Electrophoresis*; GIT Verlag: Darmstadt, Germany, 1990.
(2) Bauer, J. *Electrophoresis* **1998**, *19*, 1057–1235. (special issue)
(3) Krivánková, L.; Bocek, P. *Electrophoresis* **1998**, *19*, 1064–1074.
(4) Weber, G.; Bocek, P. *Electrophoresis* **1998**, *19*, 1649–1653.
(5) Janasek, D.; Schilling, M.; Manz, A.; Franzke, J. *Lab Chip* **2006**, *6*, 710–713.
(6) Albrecht, J. W.; El-Ali, J.; Jensen, K. F. *Anal. Chem.* **2007**, *79*, 9364–9371.
(7) Albrecht, J. W.; Jensen, K. F. *Electrophoresis* **2006**, *27*, 4960–4969.
(8) Fonslow, B. R.; Bowser, M. T. *Anal. Chem.* **2006**, *78*, 8236–8244.
(9) Kohlheyer, D.; Besselink, G. A. J.; Schlautmann, S.; Schasfoort, R. B. M. *Lab Chip* **2006**, *6*, 374–380.
(10) Kohlheyer, D.; Eijkel, J. C. T.; Schlautmann, S.; van den Berg, A.; Schasfoort, R. B. M. *Anal. Chem.* **2007**, *79*, 8190–8198.
(11) Xu, Y.; Zhang, C. X.; Janasek, D.; Manz, A. *Lab Chip* **2003**, *3*, 224–227.
(12) Zhang, C.-X.; Manz, A. *Anal. Chem.* **2003**, *75*, 5759–5766.
(13) Lu, H.; Gaudet, S.; Schmidt, M. A.; Jensen, K. F. *Anal. Chem.* **2004**, *76*, 5705–5712.
(14) Kohlheyer, D.; Eijkel, J. C. T.; van den Berg, A.; Schasfoort, R. B. M. *Electrophoresis* **2008**, *29*, 977–993.
(15) Pamme, N. *Lab Chip* **2007**, *7*, 1644–1659.

10.1021/ac800275c CCC: $40.75 © 2008 American Chemical Society
Published on Web 04/25/2008

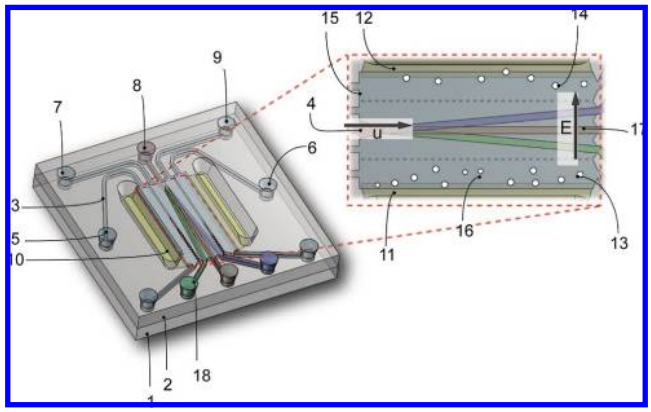

Figure 1. Schematic illustration of the microfluidic free-flow electrophoresis chip with integrated platinum electrodes. Oxygen and hydrogen bubbles generated at the electrodes disturb the separation and flow pattern. Bubble generation can be suppressed by adding adequate chemical substitutes. (1, bottom chip plate; 2, top chip plate; 3, inlet channel; 4, hydrodynamically focused sample stream; 5, inlet for anodic electrolyte; 6, inlet for cathodic electrolyte; 7, 9, inlets for carrier electrolyte sheath flows; 8, sample inlet; 10, electrode contact pad; 11, anode; 12, cathode; 13, oxygen bubble; 14, hydrogen bubble; 15, cathodic electrolyte stream; 16, anodic electrolyte stream; 17, separated component). The entire separation and electrode area has a depth of 10 μm. To distinguish between the electrode regions and the separation chamber and to allow easy chip alignment during microscopy, two rows of micropillars were implemented into the design. These pillars do not disturb or influence the device performance.

in microfluidic free-flow electrophoresis chips. In this approach, the generation of oxygen and hydrogen bubbles is suppressed by adding a redox-couple to the electrolyte flowing along the electrodes. As a first demonstration quinhydrone (QH), which is a complex between hydroquinone (H_2Q) acting as an electron donor and *p*-benzoquinone (Q) acting as an electron acceptor, was added to the flow streams at the anode and the cathode. QH is known for its application in pH sensor and related devices.[16] Instead of water oxidation and reduction, generating oxygen and hydrogen, now H_2Q is oxidized and Q is reduced without the generation of bubbles. Although this method is only applicable with low electrical current densities due to the depletion of QH, it was successfully demonstrated with fluorescent components separated in free-flow zone electrophoresis, as described here. This approach allows for a simple chip design, where the electrodes can be located directly inside the separation chamber without the need for separating structures or membranes. Although the chip design was simplified, the setup was slightly more complex since additional sheath flows were used to isolate the redox species from the analyte solution as described in the following section in more detail.

Principle. The layout and device configuration is shown in Figure 1. The device has five inlets, which are connected via capillaries to a set of syringe pumps, to allow multiple adjacent flows with different chemical composition and flow rate. Inlets 5 and 6 (see Figure 1) are used for the anodic and cathodic electrolyte flow. Only these streams contain the redox-couple QH. The sample solution is introduced via inlet 8 and is hydrodynamically focused by two parallel sheath flow streams (inlets 7 and 9). Because of this stream configuration, the sample stream is shielded from the QH containing electrolytes. Since QH is electrically neutral, cross contamination between the streams is based on diffusion only. Five outlets (shown as 18 in Figure 1) can be used to collect the separated fractions. The number of outlets does not correlate with the number of analyte fractions and was just chosen for practical reasons to allow a simple chip design.

EXPERIMENTAL SECTION

Materials and Reagents. If not otherwise stated, all chemicals were obtained from Sigma-Aldrich-Fluka. Solutions were degassed in vacuum prior to application. The carrier medium solution contained 10 mM Hepes (adjusted with 2 M NaOH to pH 7), 0.1% Tween 20, and 0.1% HPMC (chip inlets 7 and 9, see Figure 1), and was used for the hydrodynamic focusing. All other solutions were of this basic composition plus additional compounds as described in the following. The sample solution contained 0.5 mg mL^{-1} fluorescein, 0.5 mg mL^{-1} rhodamine B, and 0.5 mg mL^{-1} rhodamine 6G (in total 1.5 mg mL^{-1}) (chip inlet 8). A sample solution without rhodamine 6G was prepared additionally (chip inlet 8). Furthermore, two solutions of 2 mg mL^{-1} *p*-benzoquinone and 2 mg mL^{-1} hydroquinone, respectively, were prepared (chip inlets 5 and 6). Since the QH complex degrades within hours, the two components were prepared and mixed in a 1:1 ratio just before the experiments.

Chip Fabrication. Each chip consists of two thermally bonded Borofloat 33 glass plates (Schott Jenaer Glas, Germany); the top plate contains the channels, separation chamber, fluidic inlets and outlets, and the electrode openings, while the bottom plate contains the patterned platinum electrodes. On the top plate, hydrofluoric acid was used to etch the channels and separation chamber while a chromium−gold layer protected the regions not to be etched. The etch depth was 10 μm. A powder blasting step was performed with 30 μm in diameter Al_2O_3 particles to create the inlet and outlet holes, as well as the electrode openings.[17] A photolithography step was carried out to transfer the pattern of the electrodes onto the surface of the bottom plate. The glass was exposed for 10 min to a BHF etch to obtain a recess of 200 nm depth at the areas where the platinum would be deposited. Subsequently a 10 nm chromium adhesion layer was sputtered on top of the wafer followed by a 190 nm platinum layer.[18] A lift-off in acetone was performed, leaving the surface of the platinum electrodes level with the surface of the glass plate, so that no steps were present on the surface. This allowed direct wafer bonding to the top plate. The top and bottom glass plates were aligned by stereomicroscope and thermally bonded at 600 °C for 1 h, whereas heating up and cooling down was carried out over 12 h in total to avoid internal material stress. The bonded plates were finally diced into several microfluidic chips. For electrical connection, two wires were soldered to the platinum connections pads, with the final chip shown in Figure 2.

Experimental Setup and Methods. The fabricated chips were placed in an in-house fabricated plastic holder. Syringe pumps (CMA/102, Microdialysis, Sweden) were used to control

(16) van der Schoot, B.; Bergveld, P. *Sens. Actuators* **1985**, *8*, 11–22.

(17) Wensink, H.; Elwenspoek, M. C. *Sens. Actuators, A: Phys.* **2002**, *102*, 157–164.

(18) Schlautman, S.; Wensink, H.; Schasfoort, R.; Elwenspoek, M.; van den Berg, A. *J. Micromech. Microeng.* **2001**, *11*, 386–389.

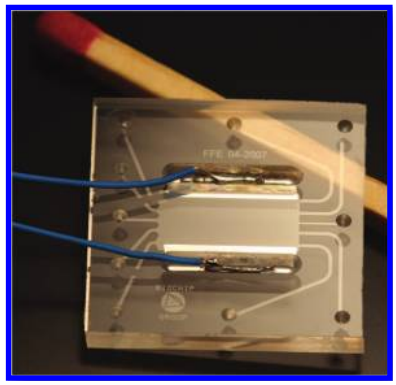

Figure 2. Photograph of the microfabricated glass free-flow electrophoresis chip with integrated platinum electrodes and soldered electrical connections. The chip size is 20 mm × 20 mm with a thickness of 2.2 mm. (separation chamber: $L \times W \times H$, 10 mm × 6 mm × 10 μm, volume = 600 nL).

the flow rates. Glass syringes (1 mL) (Microdialysis, Sweden) were filled with the required solutions and connected via glass capillaries (Aurora, The Netherlands) and Nanoport connectors (Upchurch Scientific) to the in-house fabricated chip holder. The two integrated platinum electrodes were connected to a power supply (Labsmith). Power supply and syringe pumps were controlled in real-time with a personal computer and Labview software (National Instruments). The holder was placed on an inverted microscope (Olympus IX51) equipped with a mercury burner and fluorescent filter set (XF57, Omega Optical) for fluorescence detection. Images were captured with the digital color camera ColorViewII (Olympus) and recorded with the software package AnalySIS 5 (Olympus). Intensity profiles were further analyzed using Origin (Microcal Software) to determine peak positions and standard deviations.

RESULTS AND DISCUSSION

Bubble-Free FFZE. The three fluorescent dyes fluorescein, rhodamine B, and rhodamine 6G were chosen as a set of model components to demonstrate bubble-free FFZE using QH as the redox compound. As shown in Figure 3, all three components clearly separated and followed diverging lanes at an overall flow velocity of 2 mm s^{-1}, an applied voltage of 300 V (resulting in an approximate electrical field of $E \approx 15$ V mm^{-1} across the separation region) and an average electrical current of $I \approx 20$ μA. At pH 7, rhodamine B is neutral[19] and as expected showed no deflection, while fluorescein (charge −2) moved toward the anode and rhodamine 6G (charge +1)[19] was deflected toward the cathode. The deflection d in free-flow zone electrophoresis is be described by

$$d = \mu_p E t \quad (1)$$

where μ_p is the apparent electrophoretic mobility, E is the electrical field strength, and t is the residence time of molecules in the separation chamber.[20] At a residence time of $t_r = 4$ s, the lateral deflection of fluorescein was approximately $d_{\text{fluorescein}} \approx -1$ mm,

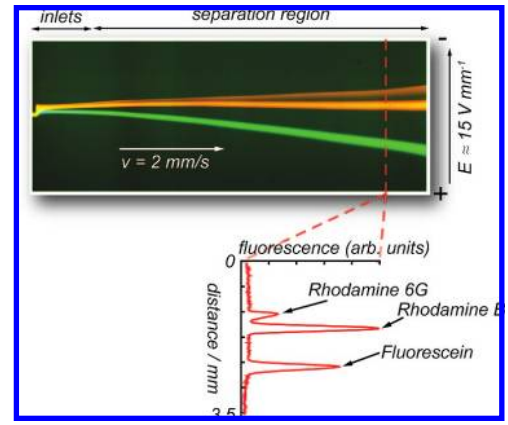

Figure 3. Image showing free-flow zone electrophoresis of three fluorescent dyes. An intensity profile was generated to demonstrate separation performance. Here, the suppression of oxygen and hydrogen bubbles enabled a stable nondistorted continuous separation. (Image contrast and colors were enhanced for better visualization.)

and the deflection of rhodamine 6G was approximately $d_{\text{rhodamine6G}} \approx +0.4$ mm.

Quinhydrone Redox-Couple. Although the position of the separated lanes was not fully stable, as discussed later, no gas bubbles appeared and distorted the separation. In the experiment shown in Figure 3 and described above, a solution of 18 mM QH was used as the electrolyte flowing along the electrodes. With a resulting electrical current of approximately 20 μA at the electrodes, instead of electrolysis of water molecules, hydroquinone was undergoing oxidization (losing electrons at the anode) and *p*-benzoquinone reduction (gaining electrons at the cathode) to enable electrical current flow. QH gets oxidized and reduced at lower potential than water molecules and without gas formation. The QH electrode reactions are given by[16]

$$\text{anodic reaction} \quad C_6H_4O_2H_2 \rightarrow C_6H_4O_2 + 2H^+(aq) + 2e^- \quad (2)$$

and

$$\text{cathodic reaction} \quad C_6H_4O_2 + 2H_2O + 2e^- \rightarrow C_6H_4O_2H_2 + 2OH^- \quad (3)$$

The addition of QH enabled a stable separation of the three components which would not be possible without. However, the transport of electrons via the oxidization and reduction of the redox active molecules hydroquinone and *p*-benzoquinone molecules is limited by their efficient mass transport toward the electrodes.[21] Since the QH complex is electrically neutral, the actual concentration of the redox-couple near the electrodes is dependent on the consumption, due to oxidization and reduction, and diffusion away from the electrodes. The diffusion distance x defined by

$$x = \sqrt{2Dt} \quad (4)$$

(19) Gear, A. R. L. *J. Biol. Chem.* **1974**, *11*, 3628–3637.
(20) Raymond, D. E.; Manz, A.; Widmer, H. M. *Anal. Chem.* **1996**, *68*, 2515–2522.
(21) Rubinstein, I., Ed., *Physical Electrochemistry*; Marcel Dekker, Inc.: New York, 1995.

and assuming a diffusion constant of hydroquinone of $D = 1 \times 10^{-9}$ m^2 s^{-1} and a maximum residence time inside the separation chamber of $t = 5$ s, the diffusion distance will be approximately 100 μm.[22] Since the diffusion distance is much larger than the electrode compartment height (10 μm), a uniform concentration can be assumed above the electrodes. With an applied electrolyte−fluid stream width (containing the redox-couple) along the electrodes of 1 mm, covering the entire electrode surface ($w = 500$ μm, $L =$ 10 mm) plus 500 μm additionally next to the electrode, it is clear that depletion of QH due to lateral diffusion can be excluded as the limiting factor. However, with an increasing electrical current, the surface concentration of QH at the electrodes downstream in the electrode compartment will decrease and eventually become zero, and H_2O molecules will start to be oxidized and reduced in addition to enabling the higher electrical current to flow. This of course will lead to gas formation again. Here we observed this effect with an electrical current between 30 and 40 μA.

In the following section, it is investigated if the current limitation is governed by the depletion of QH molecules near the electrodes. According to Faraday's law of electrolysis, the amount of electrical charges transported is proportional to the amount of molecules produced at the electrodes. In our situation this would be, e.g., the amount of hydroquinone oxidized by losing two electrons at the anode. The amount of molecules n consumed is given by

$$n = \frac{It}{zF} \tag{5}$$

where I is the electrical current over a time period t, z the number of electrons transferred per produced molecule, and $F = 96\,485$ C, the Faraday constant.[23] With eq 5 and an electrical current approximately $I_{max} = 40$ μA, a total residence time of $t = 5$ s (flow velocity $v = 2$ mm s^{-1}) and $z = 2$ (see eqs 2 and 3), one can derive $n_{con\_5s} = 10.4 \times 10^{-10}$ mol. The concentration of the QH solution was 18 mM of hydroquinone and 18 mM *p*-benzoquinone. Assuming a flow-rate of the QH solution above the electrode of $\varphi = 0.01$ μL s^{-1}, a total fluid volume of $V = 0.05$ μl passes the electrode within the residence time of $t = 5$ s. This volume contains approximately $n_{avaliable\_5s} = 9 \times 10^{-10}$ mol of hydroquinone and *p*-benzoquinone, respectively. From these calculations it is obvious that if the amount of molecules required to transport a specific electrical current exceeds the present amount of redox molecules, water molecules are oxidized and reduced instead. Occurring bubbles were observed first near the end of the electrode which makes sense considering the above considerations, since the outlet is the most redox-couple depleted region. To increase the maximum current, consequently the concentration of QH was increased. However, filming and deposition of material was observed at the electrodes and surroundings. At lower QH concentrations, e.g., c(QH) = 18 mM, no significant filming could be observed, even after several hours of experimental work. The given calculations, though reflecting only a simplified system, can suggest possible beneficial alterations to the system. It seems plausible that in order to improve the maximum current (and hence the maximum applicable separation voltage), an increase of the electrode surface area which is in contact with the electrolyte and the required redox-couple would be beneficial. For the approach presented here, no detailed investigations on the electrical current density were performed.

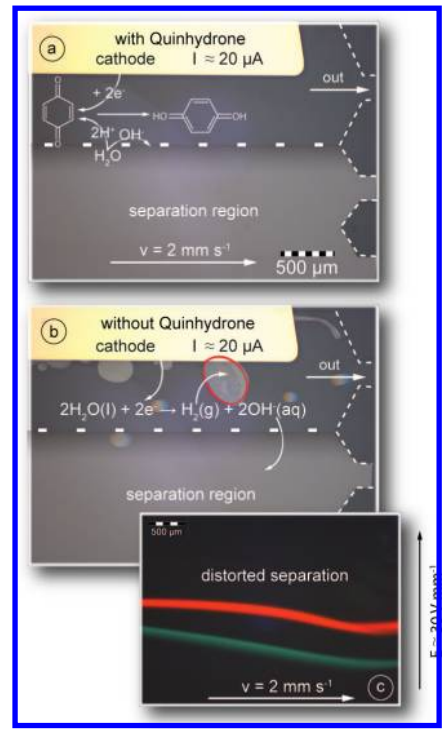

Figure 4. (a) Microscopic photograph showing the cathode and free-flow electrophoresis operations. The quinhydrone complex present in the electrolyte flowing along the cathode (and anode, not shown here) allows for bubble-free separations up to a certain electrical current. (b) When no QH is present, water molecules undergo electrolysis generating hydrogen gas bubbles at the cathode and therefore (c) disturbing the flow and separation (here separation of fluorescein and rhodamine B). For a clear visibility, the channel outlines are indicated by dotted lines and the separation region is slightly brightened.

Electrolysis of Water. Without QH added to the electrolyte solutions, electrolysis and gas bubble formation was observed when the electrical current exceeded approximately $I = 15$ μA. It is assumed that electrolysis still occurred below that value but that the gas formed at the electrodes remained dissolved in the solution. Bubbles that appeared inside the outlet channels millimeters downstream of the electrodes at lower current densities support this assumption, as presumably the water became saturated with oxygen and hydrogen inside the smaller outlet channels. Gas formation was first observed at the cathode (hydrogen) and at higher electrical currents also at the anode (oxygen). Figure 4 visualizes the problem caused by bubble generation during FFE. Figure 4a shows the absence of bubbles at the cathode during the experiments with QH, and Figure 4b shows the appearance of hydrogen bubbles at the cathode in the absence of QH. These bubbles can significantly influence the separation since they deform the local laminar flow lines. This effect is shown in the disturbance of the lanes of fluorescein and rhodamine B in Figure 4c due to a bubble formed. Obviously this can disturb the lane pattern and would reduce the separation resolution over time, e.g., when collecting fractions or monitoring

(22) Vijayan, M.; Krishnan, V. *Electroanalysis* **1995**, *7*, 197–198.
(23) Bockris, J. O. M. and Reddy, A. K. N. *Modern Electrochemistry 1-Ionics*; Plenum Press: New York, 1998.

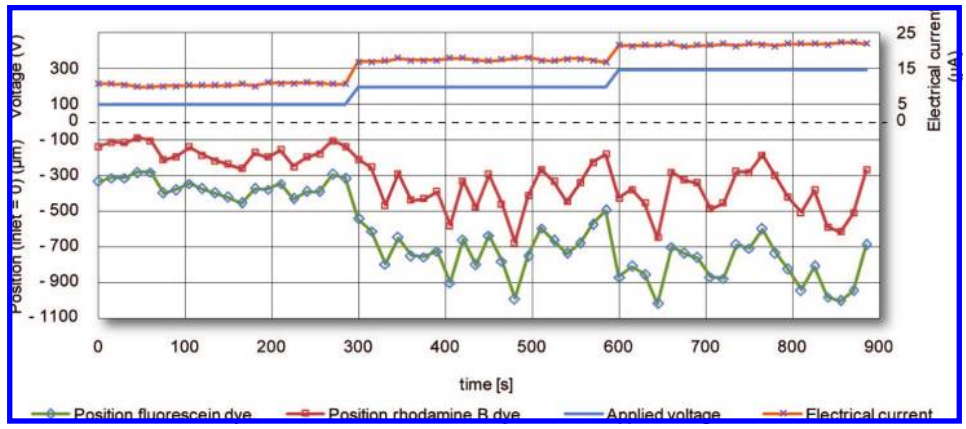

Figure 5. Diagram showing the lane position measured after a residence time of 2 s in the separation chamber in the absence of QH. Images were taken every 15 s, and peak center positions were derived of the two separated components (fluorescein and rhodamine B) over a total measurement period of 15 min. The voltage was increased from 100 to 200 V and to 300 V after 5 min, respectively. The position of the lanes was measured relatively to the sample inlet (position = 0 μm). The lane positions are strongly influenced by the gas bubbles generated at the electrodes.

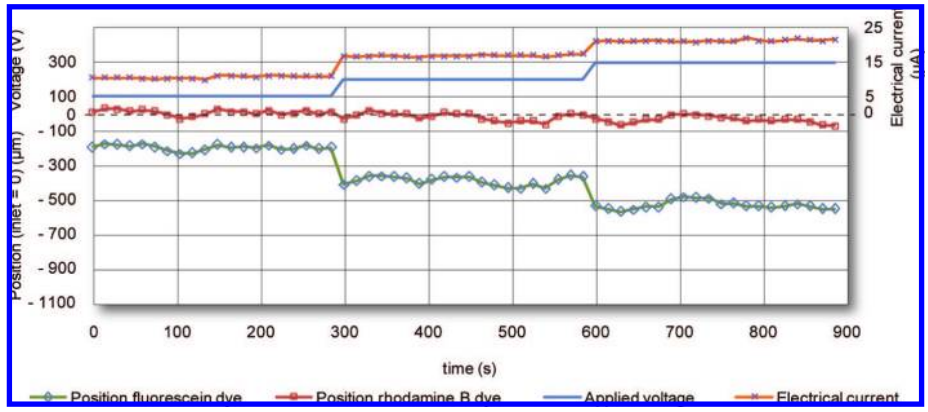

Figure 6. Diagram showing the lane position measured after a residence time of 2 s in the separation chamber in the presence of QH. Since no gas bubbles were formed at the electrodes, the effect of QH on the separation quality is clearly evident. The remaining lane fluctuations were caused by the used pumping equipment. See Figure 5 for more details.

fractions with a stationary detector. Therefore, this influence is further analyzed in the following section.

Quantitative Bubble Influence. The influence of the formation of electrolytic gas bubbles on the separation performance was investigated in more detail, particularly the impact on the separation resolution.

Two experiments were set up, one with rhodamine B and fluorescein as tracing compounds and no additional redox-couple and one experiment with added QH. During separation, microscopic images of the separated lanes of fluorescent dyes were taken and analyzed to determine the time-dependent lane positions. For this, the lane center positions of the separated dyes after a residence time of $t_r = 2$ s in the separation chamber were determined every 15 s over a period of 15 min. The voltage was set to 100 V and in 5 min intervals increased to 200 and 300 V. The results obtained are shown in Figure 5 and Figure 6, and further details are given in Table 1. The positions were measured relatively to the sample inlet which is therefore $x = 0$ μm. Deflections toward the anode were defined as negative, to allow an easier illustration. When it is referred to specific values in Table 1, in order to guide the reader, corresponding lanes and columns are indicated in brackets.

When no QH was present, as shown in Figure 5, both components fully separated. However, it is evident, that the lane positions were significantly influenced resulting in displacements as large as 500 μm, which is more than 5 times higher than the width of that lane. Furthermore, it can be seen that despite the short fluctuations, both lanes (including that of the neutral dye rhodamine B) were deflected toward the anode. From observations, we concluded that a certain amount of bubbles that remained attached to the electrodes led to a stagnant lane deflection (here between approximately 150 and 400 μm derived from the electrically neutral dye rhodamine B, see Table 1(6, a−c)). Since more hydrogen gas is formed during electrolysis than oxygen gas, most of the influence was caused by cathodic hydrogen bubbles leading here to a negative deflection. Bubbles at the anode did not tend to stick to the metal electrode and were of smaller size (up to approximately 10-fold smaller). This stagnant lane deflection might explain the slightly reduced separation distance in contrast to the results obtained with QH, see Table 1(7, a−f)). The stagnant layer of hydrogen bubbles furthermore led to an increased linear flow velocity thereby reducing the sample residence time and the migration distance (see

Table 1. Separation Pattern of Fluorescein and Rhodamine B Analyzed over 15 Minutes with and without QH[a]

				no QH			with QH		
		variable	unit	a	b	c	d	e	f
1	applied voltage	U	V	100	200	300	100	200	300
2	mean electrical current	I	μA	10.70	17.68	22.02	10.63	16.86	21.24
3	electrical field strength utilized for separation	E	V/mm	7.54	12.45	15.51	7.49	11.87	14.96
4	mobility of fluorescein (mean)	μ_f	$cm^2/V\ s$	1.42×10^{-4} ($\pm$0.1)					
5	fluorescein mean lane position	d_f	μm	−360	−707	−824	−196	−389	−530
6	rhodamine B mean lane position	d_r	μm	−168	−375	−407	9	−17	−35
7	mean separation distance ($x_r - x_f$)	d_{rf}	μm	**192**	**332**	**417**	**205**	**372**	**495**
8	separation distance standard deviation	σ_{xrf}	μm	9	16	20	4	8	10
9	fluorescein standard deviation lane position	σ_{pf}	μm	51	121	119	17	26	24
10	rhodamine B standard deviation lane position	σ_{pr}	μm	52	128	128	16	22	20
11	fluorescein standard deviation lane width	σ_{wf}	μm	51	54	62	57	63	66
12	rhodamine B standard deviation lane width	σ_{wr}	μm	50	48	52	55	54	55
13	fluorescein total standard deviation (eq 7)	σ_{pwf}	μm	72	132	134	60	68	70
14	rhodamine B total standard deviation (eq 7)	σ_{pwr}	μm	72	137	138	57	58	59
15	separation resolution single moment	Rs		**0.95 ($\pm$0.05)**	**1.63 ($\pm$0.08)**	**1.83 ($\pm$0.09)**	**0.92 ($\pm$0.02)**	**1.60 ($\pm$0.03)**	**2.05 ($\pm$0.04)**
16	separation resolution over 5 min	Rs_{5min}		**0.67 ($\pm$0.22)**	**0.62 ($\pm$0.22)**	**0.77 ($\pm$0.22)**	**0.88 ($\pm$0.07)**	**1.48 ($\pm$0.1)**	**1.92 ($\pm$0.09)**

[a] The measurements were obtained after a residence time of $t_r = 2$ s. See Limitations and Possibilities section for explanation.

eq 1). In addition to this, bubbles released from the electrodes caused short-term fluctuations of the lane positions, which can be quantified by the standard deviations given in Table 1(9,10, a−c)). These standard deviations were on the order of the lane widths (Table 1(11,12, a−c)) and higher. A common method to describe the separation efficiency for electrophoretic separation systems is the resolution R defined by

$$R = \frac{d_1 - d_2}{2(\sigma_{w1} + \sigma_{w2})} \tag{6}$$

where d_1 and d_2 are the center position of two adjacent peaks, and σ_{w1} and σ_{w2} are the corresponding standard deviations of the peak widths which here correlate to the lane widths. Except for minor variances (see Table 1(9,10, a−f)), both streams, fluorescein and rhodamine B, were equally displaced by appearing bubbles so that at a single moment in time the resolution was not affected, as shown in Table 1(15, a−f). When signals or fractions would be collected over longer periods, however, resolution (as defined by eq 6) would be greatly compromised. This can be quantified in the total standard deviation σ_{total}, including the lane width standard deviation σ_w and the standard deviation caused by the fluctuations σ_p. Adding the variances we obtain

$$\sigma_{total} = \sqrt{{\sigma_w}^2 + {\sigma_p}^2} \tag{7}$$

At 100 V, the derived resolution Rs_{5min_100V} for a sampling time of 5 min, indeed was approximately 1.4-fold lower than $Rs_{\_100V}$ for a single moment in time (Table 1(15,16, a)). With the application of 300 V, the fluctuations increased significantly resulting in a 2.4-fold decrease in resolution over 5 min (Table 1(15,16, c)). One can conclude that for practical separations and applications where, e.g., a dense array of outlet channels is used to obtain pure fractions, such fluctuations in the order of the lane width and higher are not acceptable. It has to be pointed out that fluctuations on shorter timescales than 15 s were not recorded. Since a certain number of bubbles moved with the applied flow velocity of approximately 2 mm s^{-1} spending less than 5 s in the detection window, the achieved results give only an indication of the low-frequency fluctuations and the actual variations can still be worse.

When QH was added to the electrolyte with the results shown in Figure 6, it was observed that the fluctuations were significantly reduced and that no bubbles where observed. The standard deviations of the lane center positions were roughly half of the values compared to those determined without bubble suppression at 100 V and approximately 6-fold lower at 200 and 300 V, as shown in Table 1(9,10, d−f). The remaining variance of lane position was most likely caused by the used syringe pumps, since especially the pump for the sample solution was running at the lower flow-rate limit for this pump (approximately $\varphi = 0.1\ \mu L\ min^{-1}$). This assumption is supported by the fact that fluctuations seen were independent of the applied voltage (Table 1(9,10, d−f)). It is thus concluded that this remaining source of variance can be reduced by using syringes with a smaller volume size and consequently

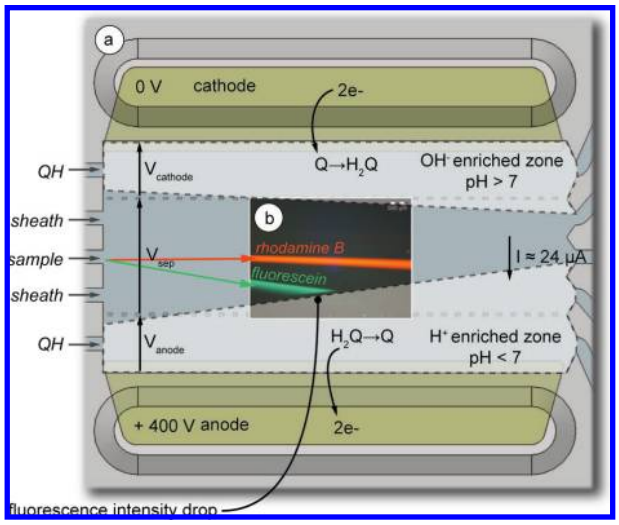

Figure 7. (a) Top view illustration of the separation chamber with electrodes with inset of (b) microscopic photograph (enhanced contrast) showing the separation of rhodamine B and fluorescein when V_{total} = 400 V were applied. Fluorescein migrated into the H^+ enriched acidic zone which caused a sudden decrease in the fluorescence emission intensity.

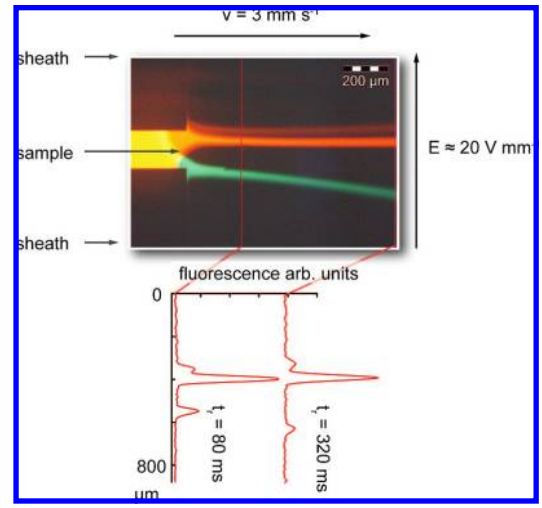

Figure 8. A microphotograph showing the rapid separation of rhodamine B, rhodamine 6G, and fluorescein below 320 ms separation time. The separation starts instantly at the sample inlet, and analytes eventually follow a linear deflection as expected.

allowing an increased piston speed. However, also the equipment-related lane fluctuations slightly influenced the resolution (see Table 1(15,16, d–f)).

As discussed, the positive effect of QH on the separation quality is evident. The separation resolution over a measurement period of 5 min for the bubble-free FFE operation was 2.5-fold higher in comparison with the device operating without QH (Table 1(16, c,f)).

Limitations and Possibilities. An important aspect to be mentioned is the variation in pH value of the carrier medium near the electrodes. As shown by the reaction equations eqs 2 and 3, QH oxidation and reduction just like water electrolysis involves the production or consumption of one proton per electron. In other FFE systems, electrodes are placed in regions with higher volume flow rates and/or larger volumes and may be strongly pH buffered to ensure stable pH values. However, in the simple chip described here, the volume of the electrode flow compartments is on the order of nanoliters and consequently slight variations in the number of H^+ or OH^- ions lead to rapid pH changes. Furthermore, because of the applied electrical field, these ions migrate toward the cathode and anode, respectively, in addition to diffusion. The consequences of this process were observed when the fluorescein lane was deflected far enough to reach the H^+ enriched acidic electrode region. The sudden drop in pH value caused a sharp decrease in the fluorescence emission intensity, as shown in Figure 7. The pH-dependent fluorescence of fluorescein is well-known, with the fluorescence practically disappearing below pH = 6.[24] Since the charge of many analytes (e.g., proteins) is highly dependent on the local pH, this would certainly affect the electromigration and thus the separation quality of these analytes. The region available for separation is therefore limited depending on flow velocity and applied voltage and buffer capacity of the QH solution. Here we found that with the application of 400 V and a flow velocity of 2 mm s^{-1}, the fluorescein band reached the linearly increasing H^+ enriched region (pH < 6) after 5 mm, which is after 2.5 s residence time as illustrated in Figure 7. The region of pH < 6 expands into the separation chamber at a rate considered to be approximately 400 μm s^{-1} (V = 400 V) due to electromigration and diffusion and approximately 300 μm s^{-1} for V = 300 V. Although not further investigated, the production of OH^- ions at the cathode will conversely lead to an enrichment of OH^- and a zone of high pH. The migration of this zone toward the separation region is assumed to be slower, due to the lower mobility and diffusion of OH^-. Despite this limitation, the device still performed well and a clear separation was achieved. As a concluding remark, it must be stated that the fabricated device with a separation chamber length of 10 mm is longer than necessary. If not necessary, the separation length, thus residence time, should be kept as low as possible, also to minimize band broadening, e.g., by diffusion.[8] In principle, separations can be performed within hundreds of milliseconds, thus completely avoiding a contamination of the separation region by chemical side products from the electrode, as shown in Figure 8, where three fluorescent dyes are separated within 320 ms. Here the separation started instantly at the sample inlet and eventually followed a linear deflection, as expected. This rapid separation demonstrates the capability of the device and indicates high miniaturization potential, since ultrarapid separations can be performed within a surface area below 1 mm^2. To be fair, it should be mentioned that the separation shown is not typical for biochemical separations since all three dyes have different charge states allowing easy electrophoretic separation.

Another observation during experimental characterization was that the system did not behave like an ohmic resistance with a linear electrical current to voltage behavior, like a stable electrolysis cell. In such a cell, depletion of ions at the electrodes and resulting concentration polarization is prevented by adding sufficient current conducting background electrolyte. In our device, only a 10 mM concentration of HEPES was present to limit the electrical current needed for operation at the required separation voltage. Hence, insufficient background electrolyte was present to prevent concentration polarization and loss of separation voltage

(24) Martin, M. M.; Lindqvist, L. *J. Lumin.* **1975**, *10*, 381–390.

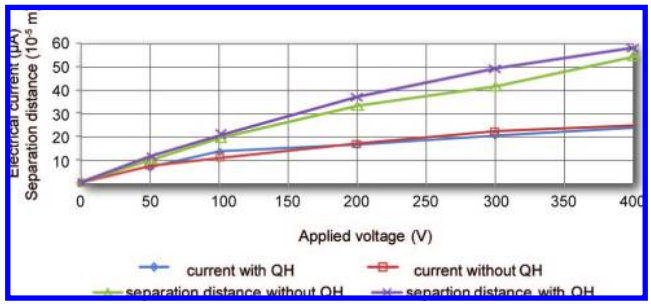

Figure 9. Diagram showing the electrical current and separation distance behavior dependent on the applied voltage. The current follows a nonlinear trend presumably due to concentration polarization at the electrodes thereby reducing the electrical field strength available for separation.

(see Figure 7, V_{sep}). This correlates with the observation that with linearly increasing the applied voltage, the electrical current did not increase linearly, as can be seen in Figure 9.

Assuming an ohmic behavior of the local separation region (without electrode regions) and constant composition and conductivity of the electrolyte inside the separation chamber (sheath + sample), the electrical resistance of the separation chamber can be calculated by

$$R = \frac{l}{\sigma A} \tag{8}$$

where l is the length (here the separation chamber width, $l = 4$ mm), σ the electrical conductivity ($\sigma_{RT} = 140\ \mu S\ cm^{-1}$), and A the cross-sectional area (height x separation chamber length, $A = 0.1\ mm^2$).[23] With eq 8, Ohm's law, and the measured electrical currents, one can derive the electrical field strength actually utilized across the separation chamber, with the results given in Table 1(3, a−f). More precise calculations of the electrical field strength across the separation region should include the conductivity changes near the sides, caused by the migrating zones of changing pH. However, as can be observed in Figure 3a, the linearity of the separation pattern was only negligibly distorted, for this reason and for simplicity a homogeneous electrical field strength along the separation chamber was assumed. With the above calculations, one can derive the mean electrophoretic mobility of fluorescein for the performed experiments applying eq 1, which results in $\mu_f = (1.42 \pm 0.1) \times 10^{-4}\ cm^2\ (V\ s)^{-1}$. This value is lower than in previous CE related publications;[25] however, the values correspond to values obtained, e.g., by Fonslow et al. with a μ-FFE device.[8] In terms of voltage efficiency,[14] as defined by the ratio of the utilized voltage for separation and the total applied voltage, the system suffers from the potential loss across the electrode regions. Here we found a voltage efficiency between 30% and 20%.

(25) Pérez-Ruiz, T.; Martínez-Lozano, C.; Sanz, A.; Bravo, E. *Chromatographia* **1998**, *48*, 263–267.

CONCLUSIONS

In this paper the bubble-free operation of a new microfluidic FFE chip with integrated platinum surface electrodes was presented. In contrast to earlier publications, electrodes were placed directly in contact with the separation medium. To avoid electrolytic bubble formation that would distort the separation lane positions, QH, a complex of hydroquinone and *p*-benzoquinone was added to the fluid streams along the electrodes for electron transfer to the solution without gas formation. This method enabled a stabilized and clear separation applying free-flow zone electrophoresis, demonstrated with a set of fluorescent dyes. A maximum electrical current between 30 and 40 μA was found before electrolysis was observed presumably due to QH depletion at the electrode surface. This value is certainly acceptable for FFE applications with low electrical currents involved. It was found that bubbles have significant influence on the separation performance as defined by the resolution. For the first time, in μ-FFE devices a long-term resolution was derived, which is of great importance for long-term signal or sample acquisition. The resolution obtained, when applying QH as bubble suppression was 2.5-fold higher than that when electrolysis was involved. The migration of H^+ ions formed at the electrodes can negatively influence the actual available width of the separation region since the low fluid volume inside the chip ($V = 600$ nL) allows quick changes in the local pH. This will be a disadvantage when separating molecules in which charge is dependent on the local pH. However, it was shown that the device is capable of separating components within tens of milliseconds residence time and a surface region below 1 mm^2, thereby totally avoiding the pH unstable region. This demonstrates the capability for further miniaturization and integration into more complex LOC systems. This is of further interest, especially where the presence of open fluid reservoirs (common in miniaturized FFE systems) and reachable electrodes should be avoided.

ACKNOWLEDGMENT

We like to acknowledge the funding of this research by the technology foundation STW. Furthermore, thanks to Hans de Boer (University of Twente, The Netherlands) for the fabrication of the chip holder and technical support and to Dr. Wout van Bennekom (University of Utrecht, The Netherlands) for his advice.

Received for review February 8, 2008. Accepted March 26, 2008.

AC800275C